Received: 29 April 2021 | Revised: 10 June 2021 | Accepted: 11 June 2021

DOI: 10.1002/jms.4775

RESEARCH ARTICLE

Journal of MASS SPECTROMETRY WILEY

Fragmentation behavior of EDTA complexes under different activation conditions

Sebastian Beck

Department of Chemistry, Humboldt-Universität zu Berlin, Berlin, Germany

Correspondence
Sebastian Beck, Department of Chemistry, Humboldt-Universität zu Berlin, Brook-Taylor-Str. 2, Berlin 12489, Germany.
Email: s.beck@chemie.hu-berlin.de

Abstract

Ethylenediaminetetraacetic acid (EDTA) is an aminopolycarboxylic acid and complexation agent that is able to bind a large variety of metals. The formation of highly stable metal-EDTA complexes is generally very quick. This has led to the use of EDTA in a variety of applications, including food, medical, and household applications. In the current study, we have investigated the fragmentation behavior of EDTA and various metal complexes under collision-induced dissociation (CID), infrared-multiphoton dissociation (IRMPD), and higher-energy collisional dissociation (HCD) activation conditions. Both, positive and negative mode electrospray ionization (ESI) were applied. The metals used to complex with EDTA ranged from alkaline earth metals, such as sodium and cesium, via calcium, nickel, zinc, aluminum, copper, iron, and indium to yttrium and several lanthanides. Furthermore, the protonated and deprotonated species of EDTA, as well as disodium and trisodium species, have been subjected to fragmentation. The results show that characteristic fragmentations were obtained for EDTA and the metal complexes under the investigated conditions. The use of an ion cyclotron resonance (ICR) and an Orbitrap mass spectrometer, as high resolution-accurate mass instruments, allowed the assignment of elemental compositions undoubtedly for the vast majority of fragments. Certain trends were observed that trend correlated with the size of the metal and the location within the periodic table.

KEYWORDS
CID, EDTA, ESI, HCD, IRMPD

1 | INTRODUCTION

Ethylenediaminetetraacetic acid (EDTA, $C_{10}H_{16}N_2O_8$), here abbreviated as H_4L with L^{4-} comprising $C_{10}H_{12}N_2O_8^{4-}$, is a chelating agent that complexes a wide range of metal ions (Me^{n+}) and was first synthesized in 1935.[1] Complexed metal ions range from all alkali metals with rather low stability constants, via all alkaline earth metals, like calcium and magnesium; transition metals like cobalt, nickel, copper, cadmium, and zinc to lanthanides and actinides.[2,3] EDTA as hexadentate ligand often forms distorted octahedral complexes with the metal ion as central atom.[4] Metal-EDTA complexes with a sevenfold coordination of the metal ion, including an extra water ligand, have also been described for Fe^{2+}, Mg^{2+}, Cd^{2+}, Co^{2+}, Mn^{2+}, Cr^{3+}, V^{3+}, Ti^{3+}, Ti^{4+}, and In^{3+}. Other metals, like Ca^{2+}, Er^{3+}, Yb^{3+}, and Zr^{4+}, even show a coordination number of eight with EDTA, including two additional water molecules. Furthermore, octahedral complexes containing a pentadentate EDTA with a non-complexed acetate group and an additional water molecule have been described for Ni^{2+}, Co^{3+},

Cu^{2+}, and Fe^{3+}.[5,6] Especially, Me^{II} and Me^{III} ions form very stable complexes, as complex formation constants (*log*K) range from 7.88 (Ba^{II}-EDTA) to 41.4 (Co^{III}-EDTA).[2]

With the extraordinarily high thermodynamic stability, EDTA is a widely used chemical in industry to complex and bind metal ions. EDTA has also been frequently used for medical purposes. Here, EDTA was applied as antidote during chelation therapies to cure metal poisoning.[7–10] Recent developments, however, avoid the use of EDTA in treatment of metal poisoning due to the inconvenience of parenteral administration and the tendency to increase the neurotoxicity of several metals.[11] In the laboratory, EDTA is most frequently employed to determine metal ion concentrations in complexometric titrations or to deactivate metal-dependent enzymes. In terms of mass spectrometric (MS) research, EDTA is often applied during metal quantification in inductively coupled plasma mass spectrometry (ICP-MS), where EDTA is utilized to bind and dissolve metal ions of interest.[12–14]

In molecular MS, EDTA is also employed to enable the detection and quantification of metal ions, which is mostly impossible with the naked Me^{n+} metal ions.[15–17] Typically, direct infusion or flow injection of mixtures for detection or quantification of complexed metal ions is performed, while the use of capillary electrophoresis-MS coupling has also been described.[18] The later was also utilized to determine EDTA levels in human plasma and urine.[19] While very specific systems, like the competitive behavior of Th^{4+} and Mn^{2+} in EDTA complexation or the simultaneous monitoring of Tl^{1+} and Tl^{3+} in a mixture with EDTA and diethylenetriaminepentaacetic acid (DTPA) have been carried out utilizing MS, more general studies with focus on the fragmentation behavior of EDTA and corresponding metal complexes are lacking.[20,21] Only a small number of studies go beyond the general detectability and investigate for instance stability constants of Cu^{2+}-, Zn^{2+}- and Ni^{2+}-EDTA by ESI-MS.[22] Barely any information is available on the fragmentation behavior of uncomplexed EDTA,[23,24] while no data on metal-EDTA complexes are available.

Here, we have investigated the fragmentation behavior of EDTA, its various sodium complexes, and a large variety of metal-EDTA complexes in positive and negative ESI ionization by collision-induces dissociation (CID), higher-energy collisional dissociation (HCD), and infrared-multiphoton dissociation (IRMPD) in combination with high resolution-accurate mass detection.

2 | EXPERIMENTAL SECTION

2.1 | Materials

Disodium ethylenediaminetetraacetic acid dihydrate (EDTA-$Na_2 \cdot 2\ H_2O$, ≥99%), $CaSO_4 \cdot 2\ H_2O$ (≥98%), $NiSO_4 \cdot 6\ H_2O$ (≥99%), $CuSO_4 \cdot 5\ H_2O$ (≥99.5%), $ZnSO_4 \cdot 7\ H_2O$ (≥99.5%), CsCl (≥99.999%), $FeCl_3$ (≥98.5%), $LaCl_3 \cdot H_2O$ (99.999%), ammonium acetate (≥97%), and formic acid (≥98%) were supplied by Carl Roth. $PrCl_3 \cdot 6\ H_2O$ (99.9%), $HoCl_3 \cdot 6\ H_2O$ (99.9%), $InCl_3$ (98%+), $YCl_3 \cdot x\ H_2O$ (99.9%), and $LuCl_3 \cdot 6\ H_2O$ (99.9%) were purchased from Alfa Aesar and $AlCl_3$ (99%), $GdCl_3 \cdot 6\ H_2O$ (99.99%), $TbCl_3 \cdot 6\ H_2O$ (99.9%), and $TmCl_3$ (99.9%) from Sigma-Aldrich. Ultrapure water (18.2 MΩ cm^{-1}) was obtained from a Millipore system (Milli-Q Plus system), and gradient grade methanol was purchased from J.T. Baker.

2.2 | Sample preparation

Metal-EDTA complexes were prepared by mixing 249 µl of a 2.5mM solution of EDTA-$Na_2 \cdot 2\ H_2O$ in 0.2 M ammonium acetate buffer (pH 8.5) with 62 µl of the corresponding metal salt solution (50 mM in water), followed by incubation for 2 h at 37°C to yield a 2 mM solution of the metal-EDTA complex. For analyses of EDTA and the different sodium-EDTA complexes (Na-EDTA (NaH_3L), Na_2-EDTA (Na_2H_2L), Na_3-EDTA (Na_3HL)), EDTA-$Na_2 \cdot 2\ H_2O$ was dissolved in 0.2 M ammonium acetate buffer (pH 8.5) to a concentration of 5 mM. Prior to measurements, all solutions were diluted 1:100 (v/v) in 50% methanol and 0.1% formic acid and directly infused into the MS.

2.3 | Mass spectrometry

Survey MS spectra, as well as CID and HCD fragmentation spectra, were acquired on an Orbitrap XL (Thermo Fisher Scientific), and IRMPD fragmentation was performed on an LTQ FT MS Ultra (Thermo Fisher Scientific), both equipped with an ESI interface. Samples were introduced at a flow rate of 5 µl min^{-1}. The ESI voltage was set to 5 kV, the sheath gas flow (nitrogen) to 15 arb, and the temperature of the transfer capillary to 230°C. Ion transfer parameters were tuned automatically for maximum intensity of the $[M+H]^+$ in positive and the $[M-H]^-$ ions in negative ion mode for all investigated complexes separately. Helium was used as collision gas in CID and nitrogen in HCD activation, correspondingly. Survey and fragmentation spectra were acquired with a resolution of 60,000 in the Orbitrap and 100,000 in the FTICR. Precursor ions were isolated with a Δm/z of 8 with the exception of Al-EDTA in positive ionization mode and Fe-EDTA in negative ionization mode (see Section 3). Normalized collision energies, IRMPD irradiation intensities, and times (ms) are given in figures (supporting information) and were adopted from previously published investigations of DOTA complexes, yielding typically about 10% of relative precursor ion intensity within the corresponding fragment spectra.[25] Activation time in CID experiments was always set to 30 ms. IRMPD and HCD fragmentation spectra have been recorded with a mass range of m/z 50–500, and CID spectra were acquired with the lowest possible m/z for the lower limit, typically restricted to 25% of the precursor ion mass due to stabilization in the ion trap and an upper m/z limit of 500.

3 | RESULTS AND DISCUSSION

3.1 | Survey spectra

The non-metal containing EDTA was easily detected in both ionization modes, yielding the $[H_5L]^+$ and the $[H_3L]^-$ ions as abundant

signals. The most abundant signal in ESI of the employed EDTA-$Na_2 \cdot 2\ H_2O$ solution was Na-EDTA $[NaH_4L]^+$ in the positive and EDTA $[H_3L]^-$ in negative ionization mode. Further signals in positive ionization were Na_2-EDTA $[Na_2H_3L]^+$ and Na_3-EDTA $[Na_3H_2L]^+$. All signals were in the same order of magnitude, while very low abundant signals for Na_4-EDTA $[Na_4HL]^+$ and Na_5-EDTA $[Na_5L]^+$ have also been observed (Figure 1A). In negative ionization mode, the observed signals for Na_2-EDTA $[Na_2HL]^-$ and Na_3-EDTA $[Na_3L]^-$ were significantly lower in intensity when compared with $[H_3L]^-$ and species containing four or five sodium have not been observed.

The Cs-EDTA mixture showed $[CsH_4L]^+$ as low abundant species, while the cesium ion $[Cs]^+$ was the most abundant ion in positive ESI here (Figure 1B). Additionally, $[CsNaH_3L]^+$ and $[CsNa_2H_2L]^+$, two species containing both cesium and sodium, were detected. In negative ESI, the unbound cesium was not detected, and the Cs-EDTA complex was mostly detected as $[CsH_2L]^-$.

The Me^{II}-EDTA (Me = Ca, Ni, Cu, Zn) complexes all showed the expected $[MeH_3L]^+$ species in positive and $[MeHL]^-$ species in negative ionization.

The Me^{III}-EDTA (Me = Al, Fe, In) complexes were also detected as $[MeH_2L]^+$ in positive and $[MeL]^-$ in negative ionization. $[AlH_2L]^+$ at m/z 317.0560 interfered with the $2 \cdot {}^{13}C$ signal of $[NaH_4L]^+$ at m/z 317.0841, so the isolation width for fragmentation experiments was lowered to one and extra care was taken when assessing corresponding fragment spectra for sum formulae. In negative ionization, this was less pronounced, as here the sodium adducts of EDTA were much lower in intensity. Iron showed the dominant formation of $[Fe^{II}HL]^-$ in negative mode. Thus, Fe^{III} in complex with EDTA, similar to Fe^{III}-DOTA, was mostly converted to Fe^{II}-EDTA under reducing negative ESI conditions.[25] For fragmentation experiments of Fe^{III}-EDTA, the isolation width was so similarly lowered to one, in order to exclude the Fe^{II}-EDTA complex from fragmentation experiments of Fe^{III}-EDTA. To exclude major abundance changes in the resulting fragment spectra that stem from the reduced isolation width, we also performed MS/MS experiments with an isolation width of $\Delta m/z = 8$ and did not observe noticeable differences in intensities of Al- and Fe^{III}-EDTA-derived fragments.

Yttrium that has been regarded as quasilanthanide throughout this manuscript and all investigated lanthanides harbor nine coordination sites. While EDTA only provides six coordination sites, complexes containing several water molecules comprise the solution form of these complexes.[26] Using ESI as soft ionization technique, ions of the form $[LnH_2L]^+$ (Ln = Y, La, Pr, Gd, Ho, Tb, Tm, Lu) and also $[LnH_2L + H_2O]^+$ have been detected in positive mode. Interestingly, no signals for $[LnH_2L+2\ H_2O]^+$ or $[LnH_2L+3\ H_2O]^+$ were detected in positive mode, indicating that the water molecules are only weakly bound. Although no steps (e.g., manipulation of source or ion transfer conditions) were undertaken to optimize the intensity of potential water adducts, the tendency for water addition was clearly visible and increased with increasing atomic number, while it was only significantly apparent among the lanthanides (Figure 2). In negative ion mode, only ions of the form $[LnL]^-$ were detected, and no water-containing ions were detected. No methanol or formic acid adducts, both present in the infused solution, were observed in any of the performed experiments.

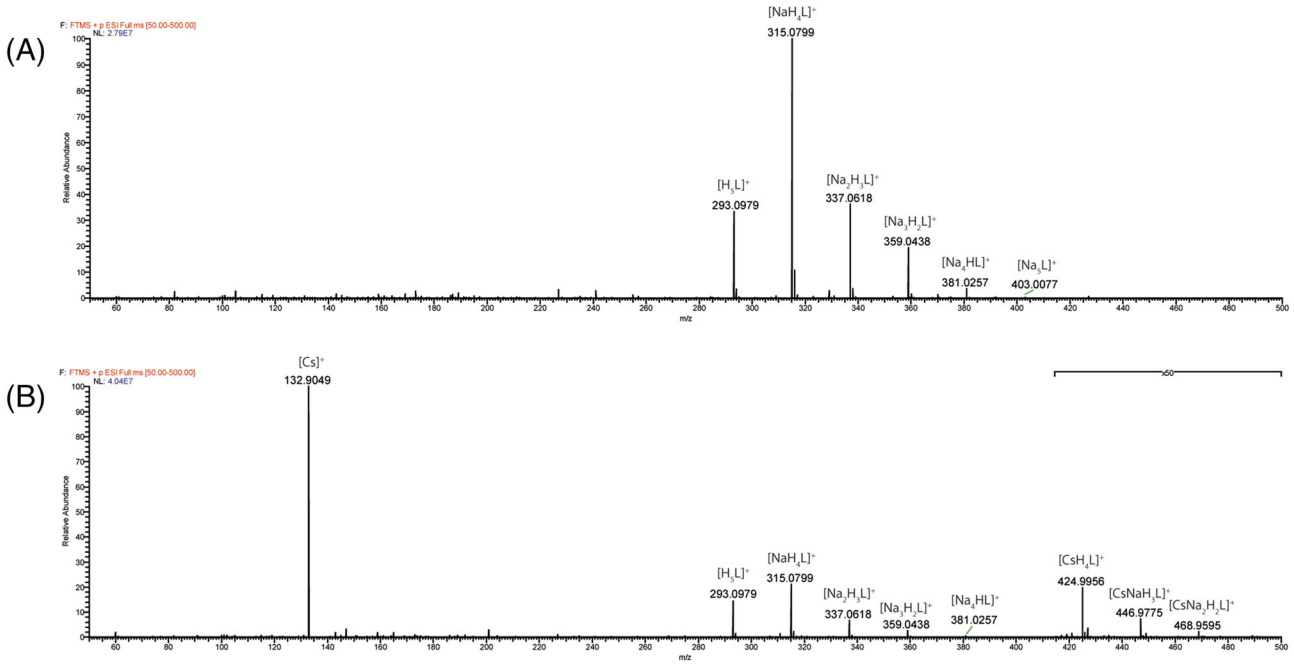

FIGURE 1 Survey spectra of (A) a solution of EDTA, showing protonated EDTA as $[H_5L]^+$ and the various sodium adducts (Na-EDTA $[NaH_4L]^+$, Na_2-EDTA $[Na_2H_3L]^+$, Na_3-EDTA $[Na_3H_2L]^+$, Na_4-EDTA $[Na_4HL]^+$, and Na_5-EDTA $[Na_5L]^+$), and (B) a mixture of CsCl and EDTA, showing the cesium ion $[Cs]^+$, the Cs-EDTA complex $[CsH_4L]^+$, and various sodium adducts. Magnification (50-fold) is given on top of the spectrum

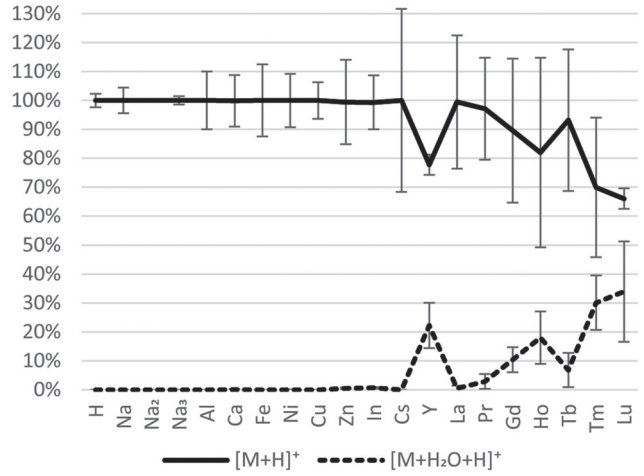

FIGURE 2 Relative proportions of $[M+H]^+$ and $[M+H_2O+H]^+$ (sum 100%) in survey spectra of EDTA and metal-EDTA complexes in positive ESI ionization

In summary, all investigated metals showed an abundant molecular ion for the corresponding metal-EDTA complex in both ionization modes. Thus, further fragmentation of all EDTA complexes could be performed utilizing CID, IRMPD, and HCD activation. All respective fragmentation schemes are shown in the supporting information, and description of fragmentation focuses on the gradual CO_2 loss channels.

3.2 | Positive CID

3.2.1 | EDTA

In the positive CID fragmentation spectra, the protonated EDTA $[H_5L]^+$ showed three abundant signals. The neutral loss of H_2CO_2 to form $[C_9H_{15}O_6N_2]^+$ was detected as main fragment here (Figure S1). Interestingly, no signal comprising the single loss of CO_2 to m/z 249.1081, omitting the extra formal H_2 loss, was detected. Further combined losses of two CO_2 and C_2H_7N or C_2H_7N and CO were also observed. Further, MS^3 fragmentation yielded losses of CO_2 and combinations of one or two CO_2, CO, and alkylamino residues from the diaminoethylene bridge of the EDTA ligand. The MS^4 yielded only losses of CO and H_2CO_2. No higher MS^N experiments were possible, due to the low abundance of fragment signals in the MS^4.

3.2.2 | Me^I-EDTA complexes

The MS/MS spectra of the sodiated $[NaH_4L]^+$ and cesium containing $[CsH_4L]^+$ EDTA were profoundly different, while both metals belong to the group of alkali metals (Figure S2). The sodium containing complex mostly showed loss of $C_2H_2O_2$ or $C_2H_2O_2$ and water. Other abundant signals in the MS/MS of $[NaH_4L]^+$ comprised to stem from losses of CO_2 or two CO_2 and C_2H_7N. In the MS/MS spectrum of $[CsH_4L]^+$, instead, only one single abundant $[Cs]^+$ signal was observed. Other signals were at least 1,000-fold less in intensity, and corresponding signals, as observed on case of sodium, were not detected at all. This behavior proved that also, in the gas phase, both complex stability constants are very different and mirror the solution stability (*log*K 1.86 for Na-EDTA and 0.2 for Cs-EDTA). Additionally, this might also reflect the highly reduced ability of cesium to bind in a multidentate conformation to EDTA due to its larger effective ionic radius (102 pm for Na^+ and 167 pm for Cs^+).[2,27] Hence, no further MS^N ($N > 2$) fragmentation of the Cs-EDTA complex could be carried out. The MS^3 of Na-EDTA resulted in losses of water, ketene, and most abundantly two CO_2 and C_2H_7N, while no MS^4 could be performed in this fragmentation channel due to the low intensities.

3.2.3 | Na_2- and Na_3-EDTA complexes

The CID MS/MS spectrum of Na_2-EDTA $[Na_2H_3L]^+$ most abundantly showed the loss of two CO_2 and H_2, among losses of $C_2H_2O_2$, three CO_2 and H_2, or combinations of CO_2 and ketene losses (Figure S3). Further fragmentation up to MS^5 yielded mostly losses of CO, CO_2, and ketene, but also ethylene. A loss of sodium was not observed in the CID spectra of Na_2-EDTA. The trisodium EDTA $[Na_3H_2L]^+$, similarly to Na_2-EDTA, most abundantly yielded the loss of two CO_2 and H_2 (Figure S4), while the corresponding single CO_2 loss signal was also present. Surprisingly, Na_3-EDTA also showed loss of CO, similar to the Me^{III}-EDTA complexes (see below), indicating that sodium acts as divalent metal here. The alternative creation of a new C—O bond to maintain the hydroxy group within the detected fragment appeared unlikely here. In the MS^3 and the higher fragmentation spectra, mainly losses of CO, CO_2, and ketene, but also alkylamino residues were observed. In contrast to Na_2-EDTA, also losses of sodium were observed that led to three remarkable species in the MS^5. These were $[ONa_3]^+$, $[HONa_2]^+$, and the radical species $[C_2H_2O_2Na_2]^{+\cdot}$.

3.2.4 | Me^{II}-EDTA complexes

The MS/MS spectra of the Me^{II}-EDTA complexes $[MeH_3L]^+$ (Me = Ca, Ni, Cu, Zn) showed a rather homogeneous picture (Figure S5). While the Zn-EDTA $[ZnH_3L]^+$ complex appeared to show the largest number of fragments, most of the signals have also been detected from the other Me^{II}-EDTA complexes with lower intensities. In general, the most abundant signals detected stemmed from losses of one or two CO_2, while both were accompanied with additional formal losses of H_2. The Cu-EDTA complex $[CuH_3L]^+$ lacked a number of signals observed for the other Me^{II} complexes, like loss of water. A unique signal was observed for the Zn-EDTA complex $[ZnH_3L]^+$, as here the abundant loss of the neutral metal to form $[C_9H_{15}O_6N_2]^+$ ($-CO_2$, $-Zn$) was observed. This behavior was unexpected, as the stability constants among the investigated Me^{II}-EDTA complexes are rather similar (*log*K 18.4 for Ni-EDTA, 18.78 for Cu-EDTA, and 16.5 for Zn-EDTA), and only the Ca-EDTA complex (*log*K 10.65 for Ca-EDTA) would be expected to potentially show such behavior from the known solution

stability constants.[2] Also, the effective ionic radii that majorly drive gas phase fragmentation behavior are similar with the exception of Ca^{2+} again (69 pm for Ni^{2+}, 73 pm for Cu^{2+}, 74 pm for Zn^{2+}, and 100 pm for Ca^{2+}) and mirror the stability constants.[27] Hence, no reasonable explanation could be given for this behavior. The MS^3 yielded a morediverse result in comparison to the MS/MS stage fragmentation. For Ca-EDTA, the loss of water was the most abundant signal here, while even a twofold loss of water was observed. For Ni-, Cu-, and Zn-EDTA the losses of CO_2 were most abundant in the MS^3. For the Ni- and Cu-EDTA complexes, a number of Me^{I} complex fragments were observed in the MS^3 spectra. These signals most likely comprised fragments of the corresponding EDTA complexes containing a Me^{I} core, while alternatively radical organic ligands bound to a Me^{II} core were possible but less likely. Interestingly, Cu^{I} organic complexes even with small ligands are well known,[28–30] but Ni^{I} complexes have so far only been described when bulky ligands are present.[31,32] In the MS^4 of the Ca- and Ni-EDTA, the breakdown of the diaminoethylene bridge of the EDTA ligand was apparent, as losses of C_2H_5N, C_2H_7N, and C_4H_9N were detected. For Zn-EDTA in the MS^4, a species comprising the loss of the neutral metal was the only abundant signal. Further fragmentation at the MS^5 and MS^6 stage manifested this behavior in case of Zn-EDTA as these spectra were dominated by metal loss species.

3.2.5 | Me^{III}-EDTA complexes

In the MS/MS spectra of the Me^{III}-EDTA complexes $[MeH_2L]^+$ (Me = Al, Fe, In) in positive ESI mode, the loss of CO_2 was most abundant for Al- and Fe-EDTA, while for In-EDTA, the loss of two CO_2 and water was the most intense signal (Figure S6). Interestingly, both Fe- and In-EDTA showed an abundant signal for $[C_7H_{12}O_9NMe]^+$ that is only possible by addition of water and loss of $C_3H_4N^{\bullet}$. Furthermore, this fragment most likely contained CO_2 directly coordinated to the Me^{II} core of the complex fragment. Otherwise, extensive rearrangement would be necessary to allow for these unusual formulae. Iron is well known for its stable 2+ oxidation state and also the direct coordination of CO_2 in case of hemoglobin CO_2 binding, while indium is not known for this behavior.[33] In the subsequent MS^N spectra, losses of CO_2, CO, and ketene but also alkylamino residues in case of In-EDTA were apparent. Al-EDTA and partially In-EDTA showed water additions in the higher MS^N spectra. As losses of CO_2 and H_2 (H_2CO_2) plus a water addition yield the same products as a CO loss, it is unclear whether the corresponding fragments originated from one or the other possibility or a combination of both. In case of formation of $[C_9H_{14/12}O_6N_2Al]^+$ and $[C_9H_{14/12}O_6N_2In]^+$ (both $-CO_2$, $+H_2O$, $(-H_2)$), the potential CO loss route could be excluded, as $[C_9H_{14}O_6N_2Me]^+$ was detected in both cases. This clearly proved the water addition combined with a loss of CO_2. Similarly, no reasonable alternative route for the formation of $[C_9H_{14}O_7N_2Al]^+$ ($-CO$, $+H_2O$) existed. The origin of this added water molecules remains unsolved, but most likely these stem from residual water in the linear ion trap in CID.

3.2.6 | Ln-EDTA complexes

As we had investigated the fragmentation behavior of lanthanide (Ln)-DOTA complexes before, we also performed similar fragmentation experiments of Ln-EDTA $[LnH_2L]^+$ (Ln = Y, La, Pr, Gd, Tb, Tm, Lu) complexes.[25] In the MS/MS spectra, all Ln-EDTA complexes showed a most dominant CO_2 loss among an additional water addition to $[C_9H_{16}O_7N_2Ln]^+$ ($-CO_2$, $+H_2O$) or loss of two CO_2 to $[C_8H_{14}O_4N_2Ln]^+$ (Figure S7). The corresponding MS^3 comprised the loss of the additionally added water. Hence, the MS^4 spectra $[C_{10}H_{14}O_8N_2Ln]^+ \rightarrow [C_9H_{16}O_7N_2Ln]^+ \rightarrow [C_9H_{14}O_6N_2Ln]^+ \rightarrow$ and MS^3 spectra $[C_{10}H_{14}O_8N_2Ln]^+ \rightarrow [C_9H_{14}O_6N_2Ln]^+ \rightarrow$ proved to be identical in all cases and showed an ambivalent behavior with respect to water addition or loss, as both species $[C_9H_{16}O_7N_2Ln]^+$ ($+H_2O$) and $[C_9H_{12}O_5N_2Ln]^+$ ($-H_2O$) were detected. Nevertheless, most dominant was the loss of a second CO_2 group here. The subsequent MS^4/MS^5 fragmentation steps again showed the loss of a single CO_2 as most abundant species for all Ln-EDTA complexes. In the $MS^{5/6}$ spectra, the starting breakdown of the diaminoethylene bridge of the EDTA ligand was observed, while once more, the loss of the last remaining CO_2 group was most abundant. Additionally, the previously observed $[H_2O_2Ln]^+$ and $[OLn]^+$ ions were observed.[25,34] Surprisingly, these were already detected during rather mild CID experiments, while previously, these hydroxide and oxide ions were only observed in HCD experiments. But again, in the background of the complex stability constants (e.g., *log*K 23.5 for Pr-DOTA and 16.3 for Pr-EDTA), this could be expected.[2]

In summary, EDTA and the various metal complexes mostly showed loss of a single CO_2 in each fragmentation step that was further accompanied by losses of water and ketene in many cases. Less frequent losses of alkylamino groups from the EDTA ligand were observed here, while for the Al- and In-EDTA complexes, as well as the Ln-EDTA complexes, frequent water additions were apparent. While the complexes of the smaller metal also yielded frequent losses of alkylamino groups, the larger metals and especially the Ln-EDTA complex spectra were dominated by CO_2 losses. Additionally, the change of metal oxidation state was observed for Ni-, Cu- and Fe- and also In-EDTA during CID fragmentation. Table 1 gives an overview of general fragmentation tendencies during positive CID activation.

3.3 | Negative CID

3.3.1 | EDTA

The fragmentation behavior of the deprotonated EDTA $[H_3L]^-$ in negative CID was similar to the positive mode fragmentation (Figure S8). The losses of water, CO_2, CO, $C_2H_2O_2$, and a combination of these formed the majority of detected ions. Surprisingly, no cleavages involving the diaminoethylene group were observed in any fragment spectrum up to MS^5, while these were already observed in the

TABLE 1 General fragmentation tendencies of selected EDTA complexes under CID activation conditions in positive and negative mode ESI ionization

		+ CID	− CID
EDTA		Losses of CO_2 and alkylamino residues	Losses of (multiple) CO_2, water, and ketene
Me^{I}-EDTA	Na^+	Losses of ketene, CO_2, and water	Losses of (multiple) CO_2, water, and ketene
	Cs^+	only $[Cs]^+$ detected	Losses of (multiple) CO_2, water, and ketene
Me^{II}-EDTA	Ca^{2+}	Losses of CO_2, ketene, and water	Losses of CO_2, water, CO, and alkylamino residues; water additions
	Ni^{2+}	Losses of CO_2, ketene, and water; detection of Ni^+ species	Losses of CO_2, water, CO, and alkylamino residues; water additions, detection of Ni^+ species
	Cu^{2+}	Losses of CO_2; detection of Cu^+ species	Losses of multiple CO_2
	Zn^{2+}	Losses of (multiple) CO_2, water, ketene, and metal	Losses of CO_2, water, CO, and metal
Me^{III}-EDTA	Al^{3+}	Losses of CO_2, CO, and ketene; water additions	Losses of CO_2, ketene, and alkylamino residues; water additions
	Fe^{3+}	Losses of CO_2 and alkylamino residues; detection of Fe^{2+} species	Losses of CO_2; detection of Fe^{2+} and Fe^+ species
	In^{3+}	Losses of multiple CO_2, CO, and alkylamino residues; detection of In^{2+} species	Losses of multiple CO_2 and ketene; detection of In^+ species
Ln-EDTA		Losses of CO_2 and water; water additions	Losses of CO_2, alkylamino residues and ketene; frequent water additions

positive MS/MS. Noteworthy was the formation of a radical species, namely, $[C_6H_{10}O_2N_2]^{-\bullet}$ in the MS^5, after loss of a methyl radical as most abundant signal that is rarely observed for even electron fragmentations.

3.3.2 | Me^{I}-EDTA complexes

The fragmentation of the Na-EDTA complex $[NaH_2L]^-$ in the negative mode MS/MS was also very similar to the positive mode (Figure S9). The dominant and sole $[Cs]^+$ signal from positive mode fragmentation of Cs-EDTA could not be observed in negative ESI mode fragmentation, due to the circumstance that positive ions cannot be detected in negative mode. Cs-EDTA instead showed a much more Na-EDTA like fragmentation behavior in negative mode. All abundant ions were observed for both $[NaH_2L]^-$ and $[CsH_2L]^-$ and showed similar intensities in the MS/MS fragment spectra. Noteworthy was the loss of the metal as hydride (−HMe) or hydroxide (−HOMe) for both Me^{I}-EDTA complexes.

3.3.3 | Na_2- and Na_3-EDTA complexes

Disodium EDTA $[Na_2HL]^-$ showed the dominant loss of CO_2, but also the loss of a sodium in the form of methyl sodium ($-CH_3Na$) (Figure S10). The corresponding MS^3 yielded a high number of signals. These included the most abundant losses of a second CO_2 group in the form of H_2CO_2, as well as losses of CO_2 and C_2H_4 or C_2H_6. Furthermore, several sodium loss species were detected. Similar to the positive CID of Na_2-EDTA, loss of CO and C_2H_2 probably led to formation of a divalent sodium core. Also, two radical species were abundantly detected for Na_2-EDTA, while only one signal comprising a water addition was apparent in the MS^5. Trisodium EDTA $[Na_3L]^-$ clearly showed a higher frequency of water additions in the negative CID MS/MS (Figure S11). Furthermore, sodium loss was already observed at the MS/MS stage. This metal loss further increased in the higher MS^N stages, as here, the majority of signals comprised loss of one or two sodium.

3.3.4 | Me^{II}-EDTA complexes

In the negative mode CID MS/MS spectra of Me^{II}-EDTA complexes $[MeHL]^-$ (Me = Ca, Ni, Cu, Zn), losses of H_2O, CO_2 (and H_2), two CO_2 (and H_2/2 H_2), and three CO_2 were abundantly detected (Figure S12). While the water loss was not detected for Cu-EDTA, it was most abundant for Ca-, Ni-, and Zn-EDTA. The loss of zinc as neutral metal, but also as hydride (H_2Zn), was detected in all higher MS^N stages of Zn-EDTA. Similar to the positive CID fragmentation, fragments containing nickel in the 1+ oxidation state after loss of $CH_3^\bullet$ or $C_3H_7^\bullet$ were detected in negative CID. This reduction in oxidation state was also observed for Cu-EDTA, albeit less frequently.

3.3.5 | Me^{III}-EDTA complexes

In the negative CID fragmentation of Me^{III}-EDTA complexes $[MeL]^-$ (Me = Al, Fe, In), exclusively, the losses of one, two, and three CO_2 were observed (Figure S13). A further MS^3 of the single CO_2 loss species resulted in the dominant cleavage of an additional CO_2 group for all metal complexes, among losses of $C_2H_2O_2$ (and H_2/2 H_2) twinned with addition of water for Al- and In-EDTA. As the signal at m/z

183.0720 for $[C_7H_{12}O_2N_2Al]^-$ was close to the most abundant $[C_6H_7O_4NAl]^-$ at m/z 184.0196, an isolation width of one had to be chosen for the MS^5 of the former in case of Al-EDTA. In this MS^5 fragmentation spectrum, numerous ions were observed. These mostly comprised loss of the last remaining CO_2 for Al-EDTA, but also losses of HCN (and H_2) and C_2H_5N. Interestingly, $[C_6H_{11}O_2NAl]^-$ had to originate by formation of a new carbon—carbon bond, as the direct binding of an alkyl residue to the Al core appeared less likely. For Fe-EDTA and In-EDTA, fragment ions containing Fe^{2+} and In^+ were abundantly observed in these MS^5 experiments.

3.3.6 | Ln-EDTA complexes

The Ln-EDTA complexes mostly showed the losses of CO_2 and additions of water in the negative CID MS/MS (Figure S14). The tendency for water addition in all these fragmentation spectra was higher than for the loss of water. Additionally, the diaminoethylene bridge was lost at an earlier MS^N stage in comparison to the positive fragmentation. Nitrogen lacking species were also observed in the higher MS^N steps of these experiments. In the MS^7, very unique species were formed. For instance $[CHO_2NLn]^-$ ($-C_2H_6$) with a HCN directly bound to the Ln^{3+} core or $[C_2H_{4/2}O_2Ln]^-$ ($-CH_3N$, ($-H_2$)) that had to contain an ethylene/acetylene residue bound to the Ln^{3+} core.

In contrast to positive CID, the tendency for multiple CO_2 losses was significantly increased during negative CID activation. Additionally, combined losses of CO_2 and water but also CO at a significantly increased rate were apparent in negative mode CID. The change of metal oxidation state was again observed for Ni-, Fe-, and In-EDTA. The Ln-EDTA complexes again showed frequent water additions, among losses of CO_2 and ketene, while the breakdown of the EDTA ligand was observed at an earlier stage in comparison to positive CID here. Table 1 gives an overview of general fragmentation tendencies during negative CID activation in comparison to the positive mode.

3.4 | Positive HCD

As HCD can only be performed as single stage activation in the employed mass spectrometer, preceding fragmentation steps were performed using CID in higher MS^N ($N > 2$) experiments. As beam-type collision activation, HCD generates multiple collisions with typically nitrogen as collision gas at an elevated pressure. Hence, more fragment ions showing a wider distribution were to be expected in HCD due to its inherent nature.[35]

3.4.1 | EDTA

HCD of the protonated EDTA $[H_5L]^+$ showed a higher tendency for CO loss in comparison to the CID fragmentation (Figure S15). Interestingly, also a radical species ($[C_7H_{12}O_4N_2]^{+\bullet}$) was observed in the MS^3 of $[C_9H_{15}O_6N_2]^+$ after loss of ketene and $H^\bullet$.

3.4.2 | Me^I-EDTA complexes

For the sodium and cesium containing Me^I-EDTA complexes $[MeH_4L]^+$ (Me = Na, Cs), only a MS/MS stage HCD experiment could be performed for Cs-EDTA (Figure S16). Identical to positive CID fragmentation, solely, a strong signal for $[Cs]^+$ was detected here. In case of Na-EDTA, the MS/MS HCD spectrum showed more complex losses. Besides the simple loss of $C_2H_2O_2$ also various combinations of cleavages of CO_2, H_2O, $C_2H_2O_2$, C_2H_7N, and $C_4H_{11/9}N$ were detected as abundant signals. Additionally, a dominant signal for the radical species $[C_6H_9N_2Na]^{+\bullet}$ (-4 CO, -3 H_2O, $-OH^\bullet$) was observed.

3.4.3 | Na_2- and Na_3-EDTA

In the positive HCD MS/MS of Na_2-EDTA $[Na_2H_3L]^+$, no dominant loss of sodium was detected (Figure S17). Instead, comparatively small fragments with low m/z values were detected. In the corresponding MS^3, most dominantly a loss of sodium was observed. In the MS^4, $[C_3H_4O_2Na_2]^+$ ($-CO_2$, $-CO$, $-C_3H_7N$) was most abundant and indicated a rather stable ion. From Na_3-EDTA $[Na_3H_2L]^+$, only MS/MS and MS^3 could be acquired in positive HCD activation (Figure S18). In the MS/MS, the most abundant loss of CO_2 and H_2CO_2 was observed, while also sodium loss species were detected. Sodium loss further became manifest in the subsequent MS^3, as here also additional signals for single and double sodium loss were observed.

3.4.4 | Me^{II}-EDTA complexes

The Me^{II}-EDTA complexes $[MeH_3L]^+$ (Me = Ca, Ni, Cu, Zn) showed a very distinct behavior to each other in positive HCD fragmentation (Figure S19). While Ca-EDTA showed the typical (multiple) CO_2, water, and alkylamino losses, Zn-EDTA mainly resulted in loss of the Zn metal core upon HCD activation. All abundant fragment ions of Cu-EDTA comprised Cu^I species and Ni-EDTA showed a hybrid behavior, as it partially formed fragment species that were detected for Ca-EDTA and the one hand, but also Ni^I species similar to Cu-EDTA on the other hand. This distinct fragmentation behavior further extended in the MS^3 and MS^4 stages of these complexes. Multiple radical species, not containing a metal core, in case of all metal complexes apart from Ca-EDTA or species with Me^I core in case of Ni- and Cu-EDTA were detected.

3.4.5 | Me^{III}-EDTA complexes

In positive HCD MS/MS of the Me^{III}-EDTA complexes $[MeH_2L]^+$ (Me = Al, Fe, In), Al-EDTA behaved similar to In-EDTA (Figure S20). These two complexes mainly yielded losses of CO, CO_2, $C_2H_2O_2$ (and H_2). For Al-EDTA, a combined ketene and CO loss was the most abundant signal in the HCD MS/MS, while the $[In]^+$ signal was most

abundant in the HCD MS/MS of In-EDTA. Fe-EDTA only showed two signals of rather complex fragmentation origin, namely, $[C_4H_{10}O_5NFe]^+$ ($-2\ CO_2$, $-C_4H_6N^\bullet$, $+H_2O$) that is only reasonably possible by addition of a water molecule due to the low carbon content and $[C_6H_{12}N]^{+\bullet}$ after loss of four CO_2 and H_2Fe. The MS^3 also revealed $[In]^+$ as most abundant signal for In-EDTA and $[C_7H_{12}O_5N_2Al]^+$ ($-C_2H_2O_2$, $+H_2O$) for Al-EDTA. The later most likely originated by addition of water and loss of ketene, rather than loss of C_2O. Fe-EDTA did not show any signals in this MS^3 or the subsequent MS^4. In the later, In-EDTA formed $[In]^+$ as most abundant and sole signal again. In the background of the complex stability constants for Al-, Fe, and In-EDTA (*log*K 16.4 for Al-EDTA, 25.0 for In-EDTA and 25.1 for Fe^{III}-EDTA), this behavior is completely unexpected but might be based on a gas phase–solution phase paradox.[2] Here, the effective ionic radii (for 53.5 pm Al^{3+}, 80 pm for In^{3+}, and 55 pm for Fe^{3+}) support the different behavior of In-EDTA, as In^{3+} might be too large for an effective multiple binding to the hexadentate EDTA.[27]

3.4.6 | Ln-EDTA complexes

The HCD fragment spectra of Ln-EDTA complexes $[LnH_2L]^+$ (Ln = Y, La, Pr, Gd, Tb, Tm, Lu) were dominated by multiple losses of CO_2 that were always accompanied by a large variety of losses of multiple hydrogens and also loss of the complete organic part of the complex (Figure S21). Figure 3 shows the comparison of CID and HCD MS/MS spectra for Pr-EDTA, where Pr-EDTA is representative for all lanthanide- and pseudolanthanide-EDTA complexes

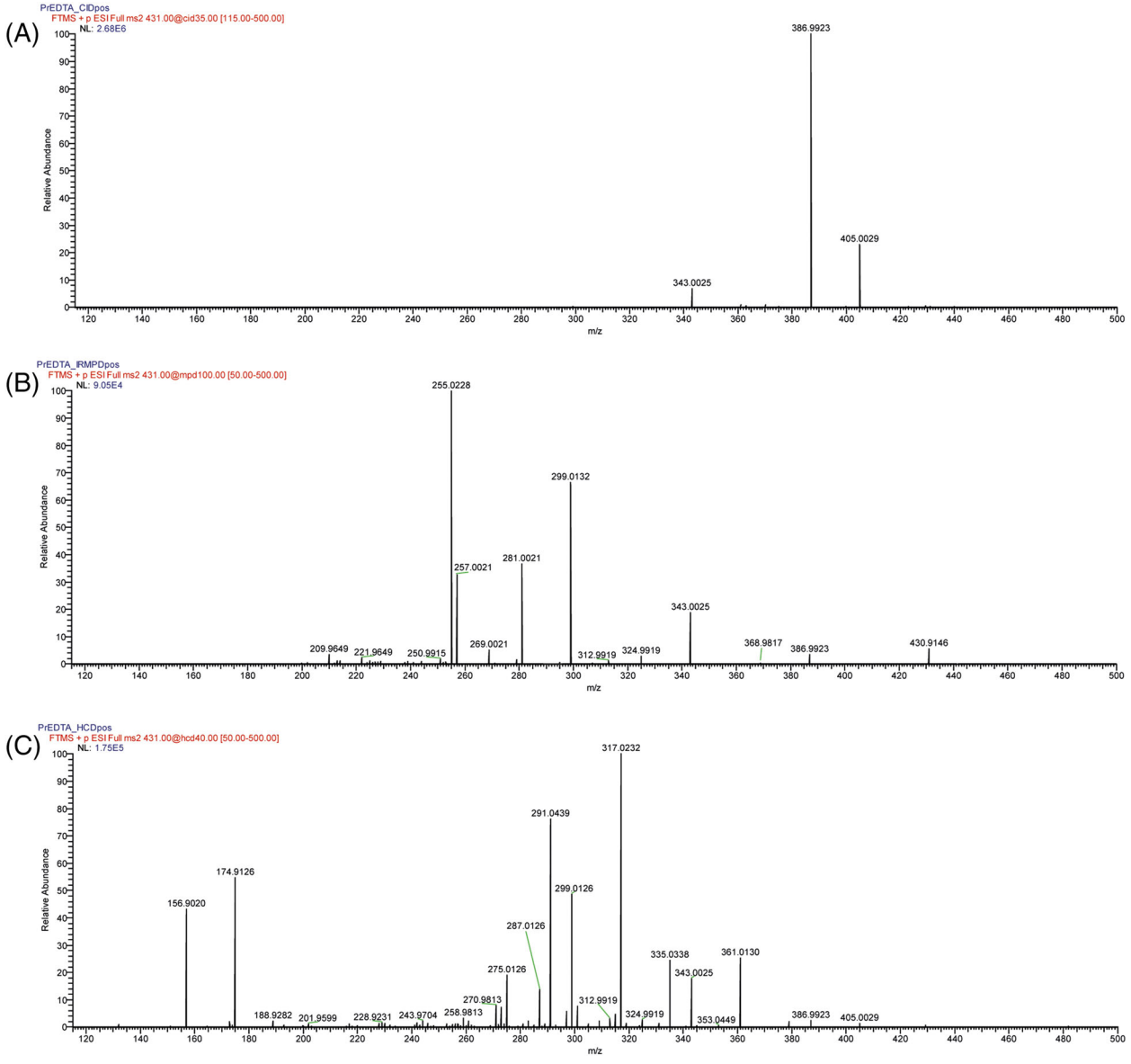

FIGURE 3 Comparison of (A) CID MS/MS, (B) HCD MS/MS, and (C) IRMPD MS/MS spectra of Pr-EDTA in positive mode ionization

showing a significantly higher number of fragments in HCD compared to CID MS/MS. The loss of the organic part of the EDTA complexes yielded the formation of $[H_2O_2Ln]^+$ and $[OLn]^+$, as previously described for Ln-DOTA complexes under HCD conditions.[25,34] Interestingly, less distinct trends for CO_2 losses and water additions have been observed among the Ln-EDTA complexes in comparison to the Ln-DOTA complexes (Figure S22).[25] The HCD fragmentation spectra of the higher MS^N stages resembled the MS/MS stage spectra in this case very much, as in the MS^3 and MS^4 stages similar signals and fragment classes were detected. Almost all carbon atoms had been lost from the complex in the fragment ions of the MS^6, while mostly lanthanide oxide and hydroxide species were detected in these spectra.

In summary, the tendency for multiple CO_2 losses and the formation of smaller m/z fragment ions in general was significantly increased during HCD in comparison to CID activation. As mentioned above, this was not unexpected based on the different mode of action of HCD in comparison to CID. Besides this tendency to fragment the EDTA ligand at earlier MS^N stages in comparison to positive CID with respect to alkyl and alkylamino losses, similar observations were made for metal oxidations states during fragmentation. While Ni-, Cu-, and Fe-EDTA showed frequent changes of oxidation state in complex with remaining parts of the EDTA ligand, In-EDTA mostly yielded $[In]^+$ as fragment ions here. The Ln-EDTA complexes showed a significantly increased tendency for water addition during HCD fragmentation. This again was in line with our previous observations of water addition among Ln-DOTA complexes, where a pressure related behavior (HCD > CID > IRMPD) was observed.[25] Table 2 gives an overview of general fragmentation tendencies during positive HCD activation.

3.5 | Negative HCD

3.5.1 | EDTA

The negative HCD MS/MS of EDTA $[H_3L]^-$ was distinct from the positive HCD or negative CID counterparts, as mostly combined losses of $C_2H_2O_2$, CO_2, and water were observed here (Figure S23). The most abundant signal was $[C_7H_{13}O_2N_2]^-$ (-3 CO_2, $-H_2$), and abundant losses of C_4H_9N in combination with two or three CO_2 were also detected. In the MS^3 and the MS^4, the fragment species $[C_3H_6O_2N]^-$ (-2 CO_2, $-C_4H_9N$ in MS^3/ $-CO_2$, $-C_4H_9N$ in MS^4) comprised the most abundant ion in both cases. Hence, this fragment species appeared to possess a comparatively stable structure.

3.5.2 | Me^I-EDTA complexes

The Me^I-EDTA complexes $[MeH_2L]^-$ (Me = Na, Cs) behaved very similar to each other in the negative HCD fragmentation (Figure S24). Both formed dominant signals of double CO_2 loss, while the majority of signals was detected for both metal complexes. Remarkably, the sodium complex appeared to be more stable than the cesium complex on the basis of the signal intensities of the metal free species $[C_3H_{6/4}O_2N]^-$ and $[C_5H_8O_2N]^-$, as both showed a comparatively higher abundance in the sodium case. This was opposing the positive HCD fragmentation spectra, where only $[Cs]^+$ was detected for Cs-EDTA indicating a very weak complex. The MS^3 negative HCD spectra were again similar to the HCD MS/MS spectra.

TABLE 2 General fragmentation tendencies of selected EDTA complexes under HCD activation conditions in positive and negative mode ESI ionization

		+ HCD	− HCD
EDTA		Losses of multiple CO_2, CO, and alkylamino residues	Losses of multiple CO_2, ketene and alkylamino residues
Me^I-EDTA	Na^+	Losses of multiple CO_2, and ketene, alkylamino residues	Losses of multiple CO_2, ketene, alkylamino residues, and metal
	Cs^+	only $[Cs]^+$ detected	Losses of multiple CO_2, ketene, alkylamino residues and metal
Me^{II}-EDTA	Ca^{2+}	Losses of multiple CO_2, water, and alkylamino residues	Losses of CO, CO_2, and alkylamino residues
	Ni^{2+}	Losses of multiple CO_2, ketene, alkyl, and alkylamino residues; detection of Ni^+ species	Losses of multiple CO_2 and alkylamino residues; detection of Ni^+ species
	Cu^{2+}	Losses of multiple CO_2, ketene, and detection of Cu^+ species	Losses of multiple CO_2 and alkylamino residues; detection of Cu^+ species
	Zn^{2+}	Loss of metal	Losses of multiple, CO, alkylamino residues, and metal
Me^{III}-EDTA	Al^{3+}	Losses of CO, CO_2, and ketene; water additions	Losses of (multiple) CO_2, CO, and alkylamino residues
	Fe^{3+}	Loss of metal; detection of Fe^{2+} species	Losses of (multiple) CO_2, CO, alkyl, and alkylamino residues; detection of Fe^{2+} species
	In^{3+}	detection of $[In]^+$	Losses of multiple CO_2, alkyl, and alkylamino residues; detection of In^+ species
Ln-EDTA		Losses of multiple CO_2 and alkylamino residues; frequent and multiple water additions	Losses of (multiple) CO_2 and alkylamino residues; frequent and multiple water additions

3.5.3 | Na_2- and Na_3-EDTA complexes

While in CID and positive HCD fragmentation spectra no or only little sodium loss was observed, in the negative HCD MS/MS of Na_2-EDTA $[Na_2HL]^-$, a large number of signals comprising sodium loss species were detected (Figure S25). Besides sodium losses, the single CO_2 loss was most abundant here. The MS^3 only showed two intense signals, both comprising a loss of sodium hydride and single and double CO_2 losses. In the MS^4, mostly single sodium species were detected and, for the first time, also complete loss of all sodium was observed, leading to the detection of numerous species not containing a sodium. A large number of fragments were detected in the negative HCD spectra of Na_3-EDTA $[Na_3L]^-$ (Figure S26). Besides water addition in combination with double CO_2 loss, mostly loss of one sodium and formations of radical species were observed in the MS/MS spectrum. In the corresponding MS^4, only two signals showed an abundant intensity. Both species only differed by the acquired water molecule and contained an unusually high number of double bond equivalents (DBEs), making newly formed carbon—carbon bonds very likely.[36]

3.5.4 | Me^{II}-EDTA complexes

The HCD fragmentation of the Me^{II}-EDTA complexes $[MeHL]^-$ (Me = Ca, Ni, Cu, Zn) was very divers among the different employed Me^{II} metals (Figure S27). This observation was similar to the positive HCD fragmentation behavior. Ca-, Zn-, and partially Ni-EDTA showed a number of signals that corresponded to the loss of CO_2, CO, and several alkylamino residues. Again, the formal loss of CO could also be achieved by loss of H_2CO_2 combined with the addition of water, while the proposed structures of the fragment ions are not affected. As there is no direct proof of water addition (e.g. increase of oxygen or hydrogen atoms during fragmentation), all affected fragmentations have been represented by loss of CO. Ni- and Cu-EDTA showed a number of Me^{I} complex fragments in these negative HCD experiments. Zn-EDTA, interestingly, did not show a dominant loss of metal from the complex here that was observed during positive HCD. The corresponding MS^3 of Me^{II}-EDTA complexes resembled the MS/MS stage. Again, the majority of signals comprised Cu^{I} species, while Ni-EDTA did not show any significant formation of Ni^{I} species. In the subsequent MS^4, Ca-EDTA did not yield any signals, and Cu-EDTA and Ni-EDTA only produced one or two low abundant signals, respectively. Most exceptional in this MS^4 of Ni-EDTA was nevertheless the formation of $[CHNNi]^-$, a complex that might contain Ni in the 1− oxidation state. However, more likely this species contained a hydride bound to Ni^{I} cyanide/isocyanide. These have so far only been described as Ni^{II} complexes bearing bulky ligands, such as triisopropylphosphine.[37]

3.5.5 | Me^{III}-EDTA complexes

The negative HCD fragmentation of the Me^{III} complexes $[MeL]^-$ (Me = Al, Fe, In) was mostly characterized by losses of CO_2 and alkyl residues (Figure S28). To our surprise, the diversity due to additional formal H_2 losses was very little in these spectra. Fe-EDTA again formed Fe^{II} complexes like $[C_6H_{9/7}O_4N_2Fe]^-$ (−2 CO_2, $-C_2H_3^{\bullet}$/$-C_2H_5^{\bullet}$), while In-EDTA showed the formation of an In^{I} complex. Although In^{III} is the most stable oxidation state of indium, In^{I} compounds and complexes have numerously been described.[38] The subsequent MS^3 could only be performed in case of Al- and Fe-EDTA, as for In-EDTA, no signals could be derived.

3.5.6 | Ln-EDTA complexes

In the negative HCD fragmentation of Ln-EDTA complexes $[LnL]^-$ (Ln = Y, La, Pr, Gd, Tb, Tm, Lu), clearly, additions of water have been proven (Figure S29). Among losses of one and two CO_2 and alkyl residues, also, alkylamino residues were lost. Most abundant for Y- and La-EDTA were $[C_9H_{14}O_7N_2Me]^-$ ($-CO_2$, $+H_2O$). For Pr-EDTA, $[C_8H_{12}O_5N_2Pr]^-$ (−2 CO_2, $-H_2$, $+H_2O$) was most abundant and $[C_6H_9O_5NLn]^-$ (−2 CO_2, $-C_2H_5N$, $+H_2O$) species were most intense for the remaining investigated Ln-EDTA complexes. The further breakdown of the complexes was observed in the subsequent MS^3, leading to a majority of signals that comprised losses of parts of the diaminoethylene bridge. All signals of significant abundance showed the addition of one or multiple water molecules, and the species $[H_4O_4Ln]^-$ was detected for all lanthanide complexes explored. Remarkable species were detected in the following MS^4. These included $[C_5H_9O_5NLn]^-$ and $[C_2H_6O_4Ln]^-$, both containing a diol functionality and $[CH_3O_3NLn]^-$ with a cyanide/isocyanide directly bound to the Ln^{3+} core. In the successive MS^5, Gd-EDTA could not be investigated. Due to the high number of Gd isotopes, the signal intensity had already been too low.

In summary and similar to the positive HCD, the tendency for formation of smaller m/z fragment ions was likewise increased in comparison to CID activation. So the tendency for multiple rather than single or double CO_2 loss was also higher in comparison to CID, and alkyl and alkylamino residues were also more frequently lost at earlier MS^N stages. The Ln-EDTA complexes showed a significantly increased tendency for water addition. This tendency was increased not only towards the negative CID counterpart, but also in comparison to the positive HCD activation. Table 2 gives an overview of general fragmentation tendencies during negative HCD in comparison to positive HCD activation.

3.6 | Positive IRMPD

As IRMPD can only be performed as single stage activation in the employed mass spectrometer, similar to HCD, preceding fragmentation steps were performed using CID in higher MS^N ($N > 2$) experiments, identical to higher stage HCD experiments.

3.6.1 | EDTA

In the positive IRMPD fragmentation of EDTA $[H_5L]^+$, only the two stages MS/MS and MS^3 could be performed for intensity reasons

(Figure S30). In the MS/MS, more ions were apparent than in the corresponding CID MS/MS, although CID is mostly regarded as very similar to IRMPD.[39,40] These comprised losses of CO and multiple CO_2 in combination with water and alkylamino residues. Furthermore, the tendency for water losses was increased in comparison to positive CID that might be related to the significant lower pressure in IRMPD in comparison to CID.

3.6.2 | Me^{I}-EDTA complexes

The cesium containing complex $[CsH_4L]^+$ behaved very similar to the CID MS/MS (Figure S31). Here again, only $[Cs]^+$ was detected in positive IRMPD activation. The sodiated EDTA complex $[NaH_4L]^+$ instead showed a contrary behavior. While in CID MS/MS mostly ketene loss was detected, in IRMPD, an additional water loss was most abundant. Furthermore, IRMPD showed lower intensities of smaller m/z values than CID. However, this observation might be caused by the inherent difficulties of ICR cells to capture small m/z ions that have not been observed for Orbitrap systems. In the corresponding MS^3 of Na-EDTA, only the loss of water was detected as abundant signal. This appeared to be a remarkably stable structure, as in the subsequent MS^4, only very weak additional signals of H_2CO_2 and ketene losses were apparent, besides the still most abundant precursor ion species.

3.6.3 | Na_2- and Na_3-EDTA complexes

The Na_2-EDTA $[Na_2H_3L]^+$ showed a similar behavior in positive IRMPD, when compared to positive CID (Figure S32). While losses of two and three CO_2 were always accompanied by H_2 losses, the most abundant signal was $[C_7H_{11}O_3N_2Na_2]^+$ ($-CO_2$, $-C_2H_2O_2$, $-H_2O$). No loss of sodium was observed here. The trisodium EDTA $[Na_3H_2L]^+$ could be assessed up to MS^4 in positive IRMPD fragmentation and showed losses of water, CO_2, $C_2H_2O_2$, two CO_2, and C_4H_9N and most abundantly losses of two CO_2 and H_2 (Figure S33). The subsequent MS^3 revealed a further breakdown of Na_3-EDTA, as most abundantly $[C_4H_5O_4NNa_3]^+$ ($-CO_2$, $-C_4H_9N$) was observed. In the MS^4, only one signal was observed that was caused by a water loss.

3.6.4 | Me^{II}-EDTA complexes

In the IRMPD MS/MS of the Me^{II}-EDTA complexes $[MeH_3L]^+$ (Me = Ca, Ni, Cu, Zn), a multitude of signals and corresponding species was detected (Figure S34). For Ca-EDTA, $[C_9H_{13}O_5N_2Ca]^+$ ($-CO_2$, $-H_2O$) was most abundant and for Ni-EDTA $[C_7H_{13}O_2N_2Ni]^+$ ($-3\ CO_2$, $-H_2$). The Zn-EDTA complex most dominantly showed loss of two CO_2 and zinc hydride to $[C_8H_{13}O_4N_2]^+$, similar to positive HCD activation. The Cu-EDTA complex yielded $[C_6H_{12}O_2N_2Cu]^+$ ($-2\ CO_2$, $-C_2H_2O_2$, $-H^\bullet$) as most abundant signal, while the majority of signals contained Cu^{I} here again. This behavior increased in the successive MS^3, as even more Cu^{I} species were detected. However, in the MS^3 also Cu^{II} species were detected. For most of the Me^{II}-EDTA complexes, similar signals as in the preceding (lower MS^N) fragmentation stages were obtained in the higher MS^N stages.

3.6.5 | Me^{III}-EDTA complexes

In the IRMPD MS/MS of the Me^{III}-EDTA complexes $[MeH_2L]^+$ (Me = Al, Fe, In), Al-EDTA did not yield any signals (Figure S35). In the positive CID MS/MS, activation of Al-EDTA resulted in losses of CO, CO_2, and H_2O. The complete lack of signals could only be explained by either of the two possibilities that the IR laser also activated formed fragment ions and as a result these further decomposed. During low energy CID in the linear ion trap (LIT), the energy is mostly transferred to the precursor ions and resulting fragments are less activated.[41,42] In case of IRMPD, Al-EDTA fragmentation might have resulted in formation of mostly $[Al]^{x+}$ ions or other small fragment ions that lay outside the possible mass range (m/z 50–500). Alternatively, the IR laser with its 10.6 μm wavelength might have stimulated the Al—N or Al—O bonds in the Al-EDTA complexes directly so that these were fully lost here. In-EDTA instead showed typical losses of $C_2H_2O_2$ (and H_2), two CO_2, and water (and H_2), with a most abundant loss of three CO_2 and water. Fe-EDTA most intensely produced $[C_6H_{12}N_2]^{+\bullet}$ ($-4\ CO_2$, $-H_2Fe$), a radical species after loss of iron (II) hydride and all carboxylic acid residues. During these experiments, we observed a severely reduced mass accuracy for fragments of Fe-EDTA during IRMPD fragmentation. During all other experiments in CID, HCD, or IRMPD, the maximum accepted error for assignment of sum formulae was 3 ppm, and typical mass accuracies were significantly below 2 ppm. With these precise analyses, it was straight forward to elemental compositions to detected signals. However, in case of Fe-EDTA, this repeatedly proved difficult with errors up to 7–8 ppm. This phenomenon could only be explained by unstable fragment ions that further decomposed during transient acquisition and so hampered the accuracy of detection. As a result, for three of the abundant signals in the IRMPD MS/MS of Fe-EDTA, several formulae seemed reasonable. Furthermore, for most of these two, corresponding fragmentation channels with distinct losses were additionally possible (Figure 4). For the detected m/z 301.9941, two compositions with a maximum mass error of 8 ppm were possible, $[C_6H_{14}O_{10}Fe]^+$ (m/z 301.9931, +3.5 ppm) and $[C_9H_{12}O_7NFe]^+$ (m/z 301.9958, −5.4 ppm). The former might have originated by loss of $C_4H_4N_2$ and addition of two water, while containing Fe^{III}. Alternatively, loss of CO_2, $C_2H_8N_2^\bullet$ and addition of four water while containing a Fe^{II} core might have been the case. $[C_9H_{12}O_7NFe]^+$ might have originated by CO_2, NH_3, and $H^\bullet$ loss plus addition of water or loss of CO and $NH_2^\bullet$. The detected m/z 273.9627 might have represented $[C_4H_{10}O_{10}Fe]^+$ (m/z 273.9618, +3.4 ppm) ($-C_6H_8N_2$, $+2\ H_2O$) or $[C_7H_8O_7NFe]^+$ (m/z 273.9645, −6.4 ppm). For formation of the second species, again, two channels were possible, either loss of CO_2, C_2H_7N, $H^\bullet$ and addition of water or loss of CO and $C_2H_6N^\bullet$. Furthermore, the detected m/z 251.9934 could have represented the species $[C_6H_{12}O_7Fe]^+$ (m/z 251.9927, +2.5 ppm) or $[C_9H_{10}O_4NFe]^+$

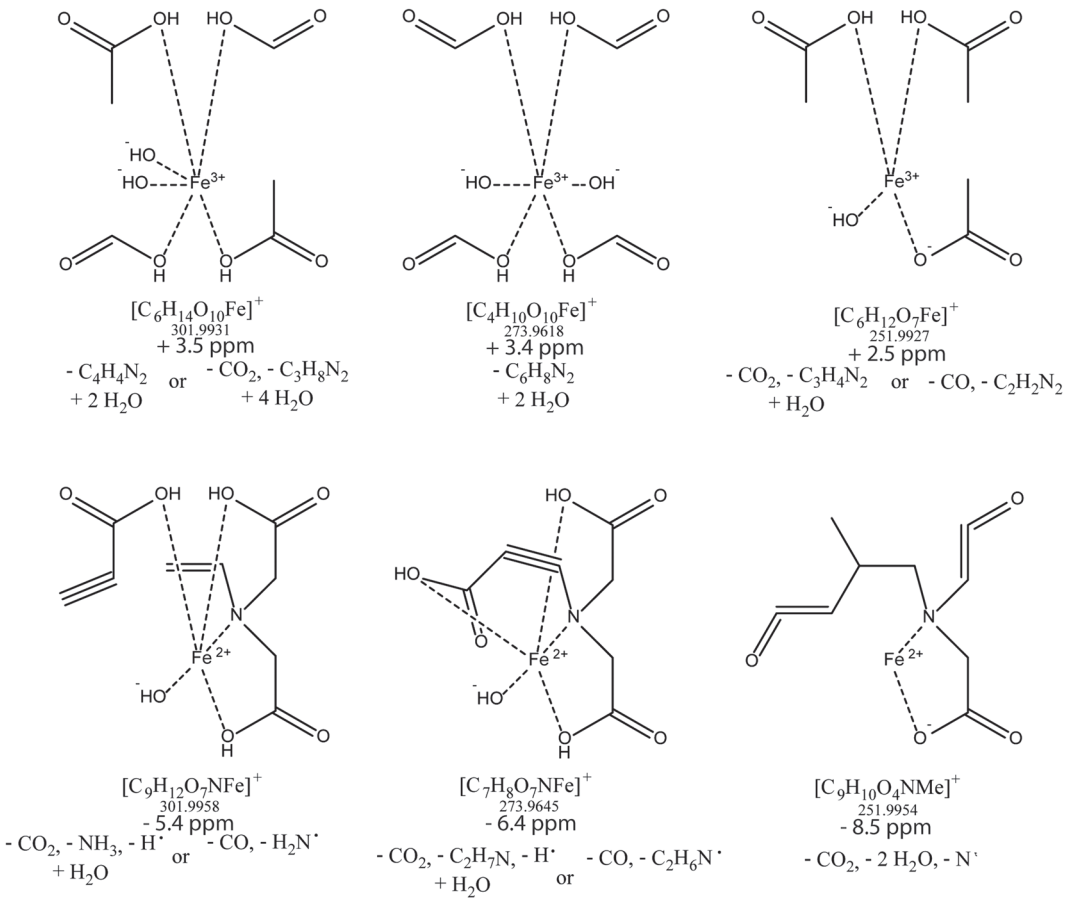

FIGURE 4 Possible structures and elemental compositions of ions detected in positive IRMPD MS/MS of Fe^{III}-EDTA. Given is the calculated mass, the observed mass error to the detected species and the possible losses from the precursor ion $[C_{10}H_{14}O_8N_2Fe]^+$ leading to the proposed structures

(m/z 251.0054, −8.5 ppm). Here, the extraordinarily high error of −8.5 ppm made is less likely that the later possibility was formed. The only possible channel by loss of CO_2, two water and a very unlikely nitrogen radical for the formation of $[C_9H_{10}O_4NFe]^+$ supported this conclusion. For the other species and signals, no definitive conclusion could be derived. However, the species involving Fe^{II} appeared more likely from a chemical point of view and in relation to the other observed fragmentations although they would involve formations of new carbon—carbon bonds or direct binding of organic residues to the Fe^{II} core. In the MS^3 of Al-EDTA, two abundant signals were observed despite the lack of signals in the MS/MS. These belonged to $[C_5H_{10/8}N_2Al]^+$ ($-CO_2$, $-C_2H_2O_2$, $(-H_2)$). Fe-EDTA again yielded the radical $[C_6H_{12}N_2]^{+\bullet}$ as most abundant signal, among other very minor mostly Fe^{III} species. In-EDTA showed a dominant loss of CO_2 and water. The corresponding MS^4 could only be performed from Fe- and In-EDTA and mostly showed losses of one or two CO_2, while Fe-EDTA again most abundantly produced $[C_6H_{12}N_2]^{+\bullet}$. The subsequent MS^5 only yielded one signals for In-EDTA. This sole signal was identified as $[C_7H_{14}O_2N_2In]^+$ ($-CO_2$).

3.6.6 | Ln-EDTA complexes

The Ln-EDTA complexes $[LnH_2L]^+$ (Ln = Y, La, Pr, Gd, Tb, Tm, Lu) showed abundant multiple losses of CO_2 (Figure S36). While the loss of three CO_2 to $[C_7H_{14}O_2N_2Y]^+$ was most abundant for Y-EDTA and the loss of three CO_2 and water to $[C_7H_{12}ON_2La]^+$ for La-EDTA, all actual lanthanides showed $[C_6H_{14}N_2Ln]^+$ (-4 CO_2) as most abundant signal. Figure 3 shows the comparison of the positive IRMPD MS/MS of Pr-EDTA to the CID and HCD equivalents that is representative for all investigated Ln-EDTA complexes. The number of abundant fragments in IRMPD MS/MS was higher in comparison to CID MS/MS, but lower than in the respective HCD MS/MS. Thus, a combination of the three activation methods would be most suited to fully characterize the fragmentation behavior of these EDTA complexes. In the subsequent MS^3, the MS/MS fragmentation behavior extended, as here also, multiple losses of CO_2 were dominantly detected. Furthermore, the beginning decomposition of the diaminoethylene bridge was apparent by losses of C_3H_5N, C_3H_7N, and C_3H_9N. Up to MS^5, no significant evidence for water addition could be detected.

$[C_6H_{16/14/12/10/8}ON_2Ln]^+$ ($-CO_2$, $+H_2O$, ($-H_2$/-2 H_2/-3 H_2/-4 H_2)) undoubtedly had acquired a water molecule due to the increasing number of hydrogen atoms from the respective precursor ion. This was the first point in positive IRMPD fragmentation of Ln-EDTA complexes where an addition of water was apparent in contrast to the other activation methods. This was easily understandable considering that IRMPD is an irradiation-based activation, not involving collision between ions or neutral gas molecules and the low pressure in the ICR cell ($\sim 2 \cdot 10^{-10}$ mbar). In the MS^6, further additions of two water were detected for most lanthanides complexes.

In summary, IRMPD showed an ambivalent behavior when compared to the other two activation methods CID and HCD. Although multiple CO_2 were often lost from the precursor ions in IRMPD that shifted IRMPD fragmentation behavior towards HCD, the tendency for water addition was significantly reduced in contrast to HCD and CID activation. Instead, a higher tendency for water losses was observed for the majority of metal complexes. This was again in line with the previously observed behavior of metal-DOTA complexes.[25] The loss of alkyl and alkylamino groups from the EDTA ligand was less often observed throughout the investigated metal complexes. Here, again, Ni^+ and Cu^+ species were detected, while In- and Fe-EDTA do not show significant changes in oxidation state as observed during positive CID and HCD. Table 3 gives an overview of general fragmentation tendencies during positive IRMPD activation.

3.7 | Negative IRMPD

3.7.1 | EDTA

In negative IRMPD, activation of the deprotonated EDTA $[H_3L]^-$ yielded loss of up to three CO_2, while the majority of intense signals contained a water loss (Figure S37). Most abundantly, the loss of two CO_2 and water has been observed. This comprised also the most intense signal in the MS^3 of EDTA, while in the MS^4, only one signal from the loss of CO_2 was detected.

3.7.2 | Me^I-EDTA complexes

In the negative IRMPD MS/MS of sodium and cesium containing EDTA complexes $[MeH_2L]^-$ (Me = Na, Cs), the combined loss of ketene and water was most abundant for Na-EDTA and the loss of two CO_2 for Cs-EDTA (Figure S38). Surprisingly, the signals for the later were not observed in the subsequent MS^3, while for both investigated metals, $[C_8H_{14}O_4N_2Me]^-$ ($-CO_2$) comprised to be the most intense signals in the MS^3. This appeared to be a very stable species in case of sodium, as it remained the most abundant signal even at increased IRMPD irradiation times up to 1,000 ms.

3.7.3 | Na_2- and Na_3-EDTA complexes

The negative IRMPD MS/MS of Na_2-EDTA $[Na_2HL]^-$ was almost identical to the negative CID MS/MS, apart from minor intensity differences (Figure S39). The MS^3 revealed losses of H_2, C_2H_6 (with a divalent sodium), and CO_2. The later was only observed in combination with H_2 or two H_2, C_2H_5N, C_4H_9N or C_2H_5N and HNa. In the MS^4, the isolated and activated precursor ion was very stable, as the IRMPD irradiation time had to be increased to 600 ms in order to obtain reasonable fragment intensities that then often comprised radical species. Trisodium EDTA $[Na_3L]^-$ yielded some unusual species upon IRMPD activation (Figure S40). While the loss of two H_2CO_2 was most abundant, $[C_7H_{8/6}O_6N_2Na_3]^-$ ($-CO_2$, $-C_2H_4$/C_2H_6) again had to contain a divalent sodium bridging two organic residues. Furthermore, the loss of sodium to $[C_5H_5O_4N_2Na]^-$ (-2 $C_2H_2O_2$,

TABLE 3 General fragmentation tendencies of selected EDTA complexes under IRMPD activation conditions in positive and negative mode ESI ionization

		+ IRMPD	− IRMPD
EDTA		Losses of multiple CO_2, water, and alkylamino residues	Losses of multiple CO_2, water, and ketene
Me^I-EDTA	Na^+	Losses of ketene and water	Losses of multiple CO_2, water, and ketene
	Cs^+	only $[Cs]^+$ detected	Losses of multiple CO_2, water, and ketene
Me^{II}-EDTA	Ca^{2+}	Losses of CO_2 and multiple water	Losses of water, CO_2, alkyl and alkylamino residues
	Ni^{2+}	Losses of multiple CO_2; detection of Ni^+ species	Losses of water, CO_2, and alkylamino residues
	Cu^{2+}	Losses of multiple CO_2 and ketene; detection of Cu^+ species	Losses of multiple CO_2 and alkylamino residues; detection of Cu^+ species
	Zn^{2+}	Losses of multiple CO_2 and metal	Losses of multiple CO_2 and alkylamino residues
Me^{III}-EDTA	Al^{3+}	Losses of multiple CO_2 and ketene	Losses of CO_2, CO, ketene, and alkylamino residues
	Fe^{3+}	Losses of multiple CO_2 and metal	Losses of multiple CO_2; detection of Fe^{2+} species
	In^{3+}	Losses of multiple CO_2, water and ketene; detection of $[In]^+$	Losses of multiple CO_2
Ln-EDTA		Losses of multiple CO_2, water and alkylamino residues	Losses of CO_2, CO and alkylamino residues; water additions

$-CH_3Na$) created a species that likely contained a sodium-bound hydrocyanic acid. In the corresponding MS^3, only one abundant group of signals $[C_8H_{10/8/6}O_4N_2Na_3]^-$ ($-CO_2$, ($-H_2/-2\ H_2/-3\ H_2$)), among numerous very minor signals was detected. The MS^4 only revealed species with a high DBE content that made the formation of new carbon—carbon bonds upon fragmentation inevitable again.

3.7.4 | Me^{II}-EDTA complexes

In the negative IRMPD MS/MS of Me^{II}-EDTA complexes $[MeHL]^-$ (Me = Ca, Ni, Cu, Zn), the loss of water was of highest intensity for Ca- and Ni-EDTA (Figure S41). For Zn-EDTA, $[C_8H_{11}O_4N_2Zn]^-$ ($-2\ CO_2$, $-H_2$) dominated the corresponding fragment spectrum. Cu-EDTA only showed two abundant signals here. Namely, the Cu^I fragment $[C_5H_9O_2NCu]^-$ ($-3\ CO_2$, $-C_2H_4N^\bullet$) and most abundantly $[C_7H_{13}O_2N_2Cu]^-$ ($-3\ CO_2$). In the subsequent MS^3, Ni-EDTA did not yield any signals, while $[C_5H_9O_2NCu]^-$ ($-2\ CO_2$, $-C_2H_4N^\bullet$) and $[C_7H_{13}O_2N_2Cu]^-$ ($-2\ CO_2$) were most and second most abundant for Cu-EDTA again. Ca-EDTA showed unusual fragmentations in the MS^3. The loss of a carbon atom to $[C_8H_{11}O_6N_2Ca]^-$ was not observed for any other metal here and the cleavage of the central diaminoethylene bridge by C_2H_4 loss was unique for Ca-EDTA as well. Zn-EDTA mostly lost CO_2 and C_4H_7N to $[C_4H_4O_4NZn]^-$. In the subsequent MS^4, Cu-EDTA did not yield any signals, but Ni-EDTA showed a most abundant loss of C_2H_5N to $[C_6H_8O_4NNi]^-$. The Zn-EDTA IRMPD MS^4 was dominated by $[C_4H_4O_4NZn]^-$ ($-C_4H_7N$) and Ca-EDTA most intensely lost H_2CO_2 to form $[C_7H_9O_2N_2Ca]^-$. The MS^5 was only possible for Ca- and Ni-EDTA and most abundantly produced loss of water for Ca-EDTA and a unique combination of losses of CH_5N, two H_2, $H^\bullet$, and addition of two water leading to the most abundant fragment $[C_6H_7O_4NNi]^-$ for Ni-EDTA. Ni-EDTA also formed the corresponding Ni^{II} species $[C_6H_8O_4NNi]^-$ ($-CH_5N$, $-2\ H_2$, $+2\ H_2O$) here. A similar Ca species, $[C_6H_6O_2NCa]^-$ ($-CH_5N$) was also observed. All these unique Ni and Ca fragments had to include a N—C carbon shift or direct binding of an alkyl residue to the metal core.

3.7.5 | Me^{III}-EDTA complexes

In the IRMPD MS/MS of Me^{III}-EDTA complexes $[MeL]^-$ (Me = Al, Fe, In), Fe- and In-EDTA mostly showed losses of two CO_2, while single and triple CO_2 losses were also observed (Figure S42). Al-EDTA most intensely yielded $[C_4H_5O_5NAl]^-$ ($-CO_2$, $-CO$, $-C_4H_7N$), while a number of signals showed a low number of DBEs. $[C_4H_7O_5NAl]^-$ ($-CO_2$, $-CO$, $-C_4H_5N$), $[C_6H_9O_4NAl]^-$ ($-2\ CO_2$, $-C_2H_3N$), and $[C_5H_7O_4NAl]^-$ ($-2\ CO_2$, $-C_3H_5N$) all formally contained a diol functionality, rather than a carboxylic acid residue. In the subsequent MS^3, this was further increased for Al-EDTA and also for In-EDTA, as $[C_4H_7O_4NAl]^-$ ($-CO_2$, $-C_4H_5N$) formally contained two and $[C_4H_5O_4NIn]^-$ ($-CO_2$, $-C_4H_7N$) or $[C_6H_{10}O_4N_2Al]^-$ ($-CO_2$, $-C_2H_2$) one diol residue. While Fe-EDTA and In-EDTA mostly showed losses of CO_2 here, Al-EDTA generally showed a higher preference to lose CO rather than CO_2 to keep the related hydroxyl group bound to the detected fragment. A further loss of CO_2 to $[C_7H_{12}O_2N_2Me]^-$ dominated the MS^4 spectra for Fe- and In-EDTA, while Al-EDTA most abundantly yielded the loss of C_2H_5N to $[C_6H_7O_4NAl]^-$. Al-EDTA again produced dominant signals that involved a loss of CO rather than CO_2. The MS^5 could only be acquired for Fe- and In-EDTA and led to the detection of only Me^{II} fragment signals for Fe-EDTA.

3.7.6 | Ln-EDTA complexes

The negative IRMPD MS/MS spectra of the Ln-EDTA complexes $[LnL]^-$ (Ln = Y, La, Pr, Gd, Tb, Tm, Lu) were characterized by most dominant losses of a single CO_2 for all Ln-EDTA complexes (Figure S43). Additionally, a number of signals undoubtedly comprising a water addition have been detected. In the subsequent MS^3, the majority of lanthanide complexes mainly showed addition of water as most abundant signal, while most fragment signals had already been detected in the former MS/MS. In the following MS^4, the majority of signals again showed an addition of water, while here, all abundant signals comprised losses of amino residues. The corresponding MS^5 could only be acquired from $[C_6H_9O_5NLn]^-$, as an activation of the corresponding threefold CO_2 loss species $[C_7H_{12}O_2N_2Ln]^-$ did not yield any signals. These MS^5 yielded a diverse picture. While for the majority of Ln-EDTA complexes the loss of ketene (and H_2) was most abundant, La-EDTA showed a most intense water loss here.

In general, negative IRMPD showed a high frequency of alkylamino losses for the investigated Me-EDTA complexes. In contrast to positive IRMPD, were mostly CO_2, ketene (and water) was lost, this higher frequency for alkylamino losses was rather similar to negative CID or HCD. Albeit observed water additions were lowest under IRMPD conditions, the Ln-EDTA complexes showed a significant amount of species that had acquired water during negative IRMPD activation. The formation of Ni^+ and Cu^+ species, frequently observed during the other activation methods, was less pronounced in negative IRMPD, while Fe-EDTA still showed the formation of Fe^{2+} species. Table 3 gives an overview of general fragmentation tendencies during negative IRMPD in comparison to positive IRMPD activation.

4 | CONCLUSION

By utilizing CID, HCD, and IRMPD, the fragmentation behavior of EDTA, its corresponding sodium complexes, and a large variety of metal complexes have been extensively investigated. The loss of the four carboxylic acid functions as carbon dioxide molecules represented the dominant and omnipresent fragmentation for EDTA and most of the investigated metal complexes. Besides, losses of ketene, carbon monoxide, and alkylamino residues were also frequently observed under all activation conditions for positive and negative ions.

The investigated Me^{II}-EDTA complexes showed the largest diversity in fragmentation behavior among the different investigated

groups here. The differences of Ca-EDTA to the remaining Me^{II} complexes were understandable due to its alkaline earth origin. The significant distinctions between Ni-, Cu, and Zn-EDTA, however, often appeared to be less straight forward. While for Ca- and Zn-EDTA, only the 2+ oxidation state was detected throughout all experiments; Cu- and also Ni-EDTA frequently showed the 1+ oxidation state. Similarly, the Me^{III}-EDTA complexes showed a divergent behavior, although less pronounced in comparison to the Me^{II} complexes. Al-EDTA had a high tendency to bind oxygen atoms mostly as hydroxide within the formed fragments, while always being detected as Al^{III} species. Iron on the other hand frequently showed Fe^{II} and partially also Fe^{I} species. Indium exhibited less activity towards changes in oxidation state. A similar behavior had been observed during our previous study on the fragmentation behavior of DOTA complexes.[25] For the investigated Ln-EDTA complexes, clearly dominant water uptakes were detected. Under non-collisional activation (IRMPD), the addition of water was less dominant, but also apparent in higher MS^N spectra. In contrast to the Ln-DOTA complexes, the Ln-EDTA complexes did not show an even oxidation state or radical species at significant abundances, as only even electron fragmentations were observed for the Ln-EDTA complexes.

In summary, for the different activation condition and polarities, a distinct fragmentation behavior of all investigated metal complexes could be proven. This was clearly visible by comparing the corresponding abundances of fragment ion intensities in the MS/MS spectra of the various complexes during CID, HCD, and IRMPD activation in positive and negative ionization mode (Figures S44–S49).

The results presented here might be exploited in further studies to further explore the gas phase chemistry of the various metal-EDTA complexes. As the proposed fragment structures are hypothetical, gas phase vibrational studies appear to be suitable to clarify the partially unique structures and also the general fragmentation behavior. Furthermore, this study might give valuable impact on quantification of EDTA and the corresponding complexes in molecular MS (e.g., ESI and MALDI), as it clearly defines potential single (SRM) and multiple reaction monitoring (MRM) pathways that are essential under low spectral resolution conditions for detection and quantification of these complexes. In summary, all EDTA complexes at first glance a showed a comparable fragmentation behavior when activated under different conditions. However, at a close examination, the differences were quite vast.

ACKNOWLEDGEMENTS

Open access funding enabled and organized by Projekt DEAL.

DATA AVAILABILITY STATEMENT

Data available in article supplementary material.

ORCID

Sebastian Beck https://orcid.org/0000-0001-6440-693X

REFERENCES

1. Paolieri M. Ferdinand Münz: EDTA and 40 years of inventions. *Bull Hist Chem*. 2017;42(2):133-140.
2. National Institute of Standards and Technology. 2004. Critically Selected Stability Constants of Metal Complexes: Version 8.0 for Windows [computer program].
3. Dean JA, Lange NA. *Lange's Handbook of Chemistry*. McGraw-Hill; 1999.
4. Harris DC. *Quantitative Chemical Analysis*. 10th ed. W.H. Freeman & Co Ltd; 2020.
5. Zubkowski JD, Perry DL, Valente EJ, Lott S. A seven coordinate co-EDTA complex. Crystal and molecular structure of aquo (ethylenediamine triacetatoacetic acid)cobalt (III) dihydrate. *Inorg Chem*. 1995;34:6409-6411.
6. Douglas BE, Randanovic DJ. Coordination chemistry of hexadentate EDTA-type ligands with M (III) ions. *J Coord Chem Rev*. 1993;128(1-2): 139-165.
7. Ferrero ME. Rationale for the successful management of EDTA chelation therapy in human burden by toxic metals. *Biomed Res Int*. 2016; 2016:1-13. https://doi.org/10.1155/2016/8274504
8. Glicklich D, Shin CT, Frishman WH. Heavy metal toxicity in chronic renal failure and cardiovascular disease: possible role for chelation therapy. *Cardiol Rev*. 2020;28(6):312-318.
9. Chisolm LL Jr. The use of chelating agents in the treatment of acute and chronic lead intoxication in childhood. *J Pediatr*. 1968;71(1):1-38.
10. Alessandro F, Maria Elena F. EDTA chelation therapy for the treatment of neurotoxicity. *Int J Mol Sci*. 2019;20(5):1019-1035. https://doi.org/10.3390/ijms20051019
11. Aaseth J, Skaug MA, Cao Y, Andersen O. Chelation in metal intoxication—principles and paradigms. *J Trace Elem Med Biol*. 2015; 31:260-266.
12. Robotti E, Quasso F, Manfredi M, et al. Determination by ICP-MS and multivariate data analysis of elemental urine excretion profile during the EDTA chelation therapy: a case study. *J Trace Elem Med Biol*. 2020;62:126608. https://doi.org/10.1016/j.jtemb.2020.126608
13. Chen Z, Sun Q, Xi Y, Owens G. Speciation of metal-EDTA complexes by flow injection analysis with electrospray ionization mass spectrometry and ion chromatography with inductively coupled plasma mass spectrometry. *J Sep Sci*. 2008;31(21):3796-3802.
14. Gallagher PA, Schwegel CA, Wei X, Creed JT. Speciation and preservation of inorganic arsenic in drinking water sources using EDTA with IC separation and ICP-MS detection. *J Environ Monit*. 2001;3(4): 371-376.
15. Baron D, Hering JG. Analysis of metal-EDTA complexes by electrospray mass spectrometry. *J Environ Qual*. 1998;27(4):844-850.
16. Stewart II. Electrospray mass spectrometry: a tool for elemental speciation. *Spectrochim Acta B*. 1999;54(12):1649-1695.
17. Urabe T, Tsugoshi T, Tanaka M. Characterization of aluminum species with nitrate, perchlorate and sulfate ions in the positive and negative ion mode by electrospray ionization mass spectrometry. *J Mass Spectrom*. 2009;44(2):193-202.
18. Quirino JP, Haddad PR. Separation and sweeping of metal ions with EDTA in CZE-ESI-MS. *J Sep Sci*. 2011;34(20):2872-2878.
19. Sheppard RL, Henion J. Quatitative capillary electrophoresis/ion spray tandem mass spectrometry determination of EDTA in human plasma and urine. *Anal Chem*. 1997;69(15):2901-2907.
20. Reinoso-Maset E, Worsfold PJ, Keith-Roach MJ. Evaluation of electrospray ionisation mass spectrometry as a technique for the investigation of competitive interactions: a case study of the ternary Th-Mn-EDTA system. *Rapid Commun Mass Spectrom*. 2012;26(23): 2755-2762.
21. Zembrzuska J, Karbowska B. Identification of complexes involving thallium(I) and thallium (III) with EDTA and DTPA ligands by electrospray ionization mass spectrometry. *Rapid Commun Mass Spectrom*. 2017;31(21):1785-1792.

22. Boija S, Almesaker A, Hedenstrom E, Bylund D, Edlund H, Norgren M. Determination of conditional stability constants for some divalent transition metal ion-EDTA complexes by electrospray ionization mass spectrometry. *J Mass Spectrom*. 2014;49(7):550-556.
23. El-Naggar SA, El-Said KS, Othman S, Mansour F, Kabil DI, Khairy MH. Cooking with EDTA reduces nutritional value of Vicia faba beans. *Biotechnol Rep*. 2019;22:e00322. https://doi.org/10.1016/j.btre.2019.e00322
24. Lowe R, Go EP, Tong GC, Voelcker NH, Siuzdak G. Monitoring EDTA and endogenous metabolite biomarkers from serum with mass spectrometry. *Spectroscopy*. 2005;19(3):137-146.
25. Beck S, Trog S, Knizia S, Linscheid MW. Fragmentation behavior of DOTA complexes under different activation conditions. *J Mass Spectrom*. 2017;52(7):442-451.
26. Conelly NG, Damhus T, Hartshorn RM, Hutton AT. *Nomenclature of Inorganic Chemistry: IUPAC Recommendations 2005*. Cambridge: Royal Society of Chemistry Publishing; 2005.
27. Shannon RD. Revised effective ionic radii and systematic studies of interatomie distances in halides and chaleogenides. *Acta Crystallogr*. 1976;A32:751-767.
28. Giri R, Hartwig JF. Cu(I)-amido complexes in the Ullmann reaction: reactions of Cu(I)-amido complexes with iodoarenes with and without autocatalysis by CuI. *J am Chem Soc*. 2010;132(45):15860-15863.
29. Li ST, Braun-Cula B, Hoof S, Limberg C. Copper(i) complexes based on ligand systems with two different binding sites: synthesis, structures and reaction with O2. *Dalton Trans*. 2018;47(2):544-560.
30. Rach SF, Kuhn FE. Nitrile ligated transition metal complexes with weakly coordinating counteranions and their catalytic applications. *Chem Rev*. 2009;109(5):2061-2080.
31. Lin CY, Power PP. Complexes of Ni(i): a "rare" oxidation state of growing importance. *Chem Soc Rev*. 2017;46(17):5347-5399.
32. Somerville RJ, Odena C, Obst MF, Hazari N, Hopmann KH, Martin R. Ni(I)–alkyl complexes bearing phenanthroline ligands: experimental evidence for CO_2 insertion at Ni(I) centers. *J am Chem Soc*. 2020;142(25):10936-10941.
33. Waterhouse J, Campbell I. Respiration: gas transfer. *Anaesth Intensive Care Med*. 2005;6(11):363-366.
34. Esteban-Fernandez D, El-Khatib AH, Moraleja I, Gomez-Gomez MM, Linscheid MW. Bridging the gap between molecular and elemental mass spectrometry: higher energy collisional dissociation (HCD) revealing elemental information. *Anal Chem*. 2015;87(3):1613-1621.
35. Ickert S, Riedel J, Beck S, Linscheid MW. Negative nucleotide ions as sensitive probes for energy specificity in collision-induced fragmentation in mass spectrometry. *Rapid Commun Mass Spectrom*. 2018;32(7):597-603.
36. Badertscher M, Bischofberger K, Munk ME, Pretsch E. A novel formalism to characterize the degree of unsaturation of organic molecules. *J Chem Inf Comput Sci*. 2001;41(4):889-893.
37. Imoto H, Moriyama H, Saito T, Sasaki Y. Synthesis of cationic hydride and related complexes of palladium and nickel with tricyclohexylphosphine or triisopropylphosphine. *J Organomet Chem*. 1976;120(3):453-460.
38. Pardoe JA, Downs AJ. Development of the chemistry of indium in formal oxidation States lower than +3. *Chem Rev*. 2007;107(1):2-45.
39. Little DP, Speir JP, Senko MW, O'Connor PB, McLafferty FW. Infrared multiphoton dissociation of large multiply charged ions for biomolecule sequencing. *Anal Chem*. 1994;66(18):2809-2815.
40. Sleno L, Volmer DA. Ion activation methods for tandem mass spectrometry. *J Mass Spectrom*. 2004;39(10):1091-1112.
41. Bayat P, Lesage D, Cole RB. Ion activation in tandem mass spectrometry using ultra-high resolution instrumentation. *Mass Spectrom Rev*. 2020;39(5-6):680-702.
42. Xia Y, Liang X, McLuckey SA. Ion trap versus low-energy beam-type collision-induced dissociation of protonated ubiquitin ions. *Anal Chem*. 2006;78(4):1218-1227.

SUPPORTING INFORMATION

Additional supporting information may be found online in the Supporting Information section at the end of this article.

How to cite this article: Beck S. Fragmentation behavior of EDTA complexes under different activation conditions. *J Mass Spectrom*. 2021;56(7):e4775. https://doi.org/10.1002/jms.4775